

Green photoluminescence mechanism in ZnS nanostructures

Haitao Chen · Yipei Hu · Xianghua Zeng

Received: 1 October 2010/Accepted: 2 December 2010/Published online: 14 December 2010
© Springer Science+Business Media, LLC 2010

Abstract ZnS Nanostructures, including nanoparticles and nanospheres, were synthesized through solvothermal process. The size and crystallinity of the ZnS nanostructures were easily controlled by the precursor source and the solvents. The photoluminescence (PL) in the range of 400–650 nm has been observed and the broad band is peaked at about 525 nm. The PL intensity reduced greatly with increasing the nanoparticle size of the as-prepared samples and the ratio of zinc and sulfur sources in the preparation process. Spectral examinations and analyses reveal that the 525 nm emission peak indeed originates from the electronic states determined by the zinc vacancies.

Introduction

As one of the most important II–VI group semiconductors, zinc sulfide (ZnS) with a wide direct band gap of 3.6–3.8 eV has been extensively investigated and used in luminescent devices, flat panel displays, infrared windows, sensors, and lasers [1, 2]. During the past few years, many ZnS nanostructures, including nanowires (nanorods), nanotubes, nanodiskettes, and nanoribbons (nanobelts) have been successfully synthesized and their photoluminescence (PL) properties have been explored [3–11]. However, the PL origin is currently still unclear and controversial due to its sensitivity to surface states, mirror

changes of electronic configurations, and preparation conditions. Generally, ZnS nanostructures show a broad PL band centered in the range of 420–450 nm and a near band gap PL band at 340 nm [3, 4]. Another often observed emission band is located at 500–550 nm. This green emission band was frequently attributed to originate from growth-related Au impurities or elemental sulfur species on the ZnS surface [5, 6]. However, controversy remains regarding the assignment of the origin of this green emission from ZnS nanostructures. For examples, Dunstan et al. [7] systematically studied the photochemistry of ZnS colloids, and assigned a green PL band at 560 nm to elemental S species on the surface of ZnS particles. Jiang et al. [8] proposed that the green band from their ZnS nanobelts came from some defect states. However, they provided no more evidence supporting their assignment. Qi et al. [9] and Zhao et al. [10] ascribed the green PL band to co-doping with copper and aluminum. Recently, Tsuruoka et al. [11] studied the green emission properties of ZnS nanobelts and found that the emission is related to line or planar defects of the ZnS nanobelts, but the defect nature is still unknown. Therefore, more investigations, concerning compositional, structural, and optical properties of nanostructural ZnS are imperative for researchers to acquaint further insight on the origins of the green PL band.

In this article, ZnS nanoparticles and nanospheres with different sizes and crystallinity have been successfully fabricated via solvothermal method. The authors carefully examine the green PL properties of the ZnS nanoparticles and nanospheres in the range of 400–650 nm and infer experimentally that the green PL is closely related to zinc vacancies. Combining with the structure analysis the authors conclude that the green band originates from an optical transition between energy levels produced by a combined zinc-vacancy defect. This study presents a

H. Chen · Y. Hu · X. Zeng (✉)
College of Physics Science and Technology, Yangzhou
University, 225002 Yangzhou, People's Republic of China
e-mail: xhzeng@yzu.edu.cn

H. Chen
National Laboratory of Solid State Microstructures, Nanjing
University, 210093 Nanjing, People's Republic of China

possible origin of the green PL band in various ZnS nanostructures.

Experiments

ZnS nanostructures with different sizes were synthesized by solvothermal process. A closed cylindrical Teflon-lined stainless steel chamber with 50 ml capacity was used for the synthesis. All the chemicals were of analytical grade and were used without any further purification. An appropriate amount of zinc acetate $[Zn(CH_3COO)_2]$ and sodium sulfide (Na_2S) were used as the zinc source and sulfur source. And the as-prepared sample is marked as sample A_0 . The as-prepared sample with zinc nitrate $[Zn(NO_3)_2]$ and sodium sulfide (Na_2S) used as the zinc and sulfur source is marked as sample B_0 . In order to analyze the influence from sulfur source, another group sample with zinc acetate and thiourea $[SC(NH_2)_2]$ as zinc and sulfur source, respectively, was also made (marked as sample C_0). The zinc and sulfur source were taken in 1:1.2 M ratios in the Teflon-lined chamber and was then filled with a chosen solvent up to 60% of its volume. After stirring for a few minutes, the closed chamber was placed inside a box furnace maintained at 160 °C for 12 h and then cooled down to room temperature. The resulting white precipitates were filtered off and washed several times using DI water and ethanol. The white powder was obtained after dried in vacuum at 60 °C for 8 h. It is noticed that the size and crystallinity of the ZnS nanostructures were dependent on many parameters such as the amount of precursor source, nature of the solvents, and reaction temperature. Most importantly, the difference in solubility of the precursor sources in a particular solvent was the significant factor determining the size of ZnS nanostructures. In this reaction process, the experimental parameters were tuned to get ZnS nanostructures with desired size and crystallinity.

The X-ray diffraction patterns of the products were measured on a German Bruker AXS D8 ADVANCE X-ray diffractometer with Cu K α radiation ($\lambda = 0.154$ nm) and a scanning speed of 0.02 s^{-1} . PL studies were carried out using a Britain Renishaw Invia micro-Raman spectrophotometer at room temperature with a 325 nm line of He–Cd laser as the excitation light source. Field emission scanning electron microscope (FESEM) images were taken on a Japan Hitachi S-4800 FESEM.

Results and discussion

Figure 1 shows the XRD patterns of as-made samples. As one can see, all the diffraction peaks can be indexed well to those of a cubic zinc blende-structured ZnS crystal with

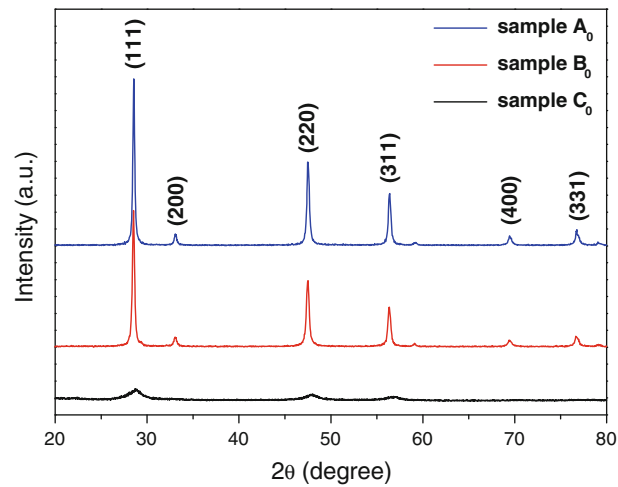


Fig. 1 XRD patterns of samples A_0 , B_0 , and C_0

lattice constants $a = 0.5406$ nm [Joint Committee Powder Diffraction Standard (JCPDS) data file Card (No 05-0566)]. No characteristic peak associated with other crystalline forms was detected in the XRD patterns. It suggests that the products are of pure crystalline phase of ZnS and other phases should be below the detection limit of the XRD. The XRD pattern shows the ZnS samples have a strongest (111) plane diffraction. It can be seen that the samples A_0 and B_0 show a stronger XRD intensity than the sample C_0 , while the sample C_0 shows the broadest reflection peaks. The difference can be understood if the authors consider the reaction mechanism. As it was mentioned in the experiment part, the samples A_0 and B_0 are directly nucleated through the reaction between the Zn ion and the free S radicals in an aqueous medium, while the sample C_0 are nucleated through medial process. In the experiments, the free sulfur radicals are released through the hydrolysis of thiourea in an aqueous medium in the Teflon cup. Then the free S radicals react with the Zn^{2+} ions to form ZnS nuclei [12], which leads to a poor crystallinity and more defects in sample C_0 . The broadest reflection peak for sample C_0 in the three samples also indicates the smallest particle size. The as-prepared ZnS nanoparticle size can be calculated by Scherrer equation: $D_{hkl} = \frac{k\lambda}{\beta_{hkl} \cos \theta_{hkl}}$, where D_{hkl} represents particle size (unit nm) as measured perpendicular to the reflecting plane (hkl). β_{hkl} is the full width at half maximum (FWHM) of X-ray diffraction peaks in radians. θ_{hkl} is diffraction angle. λ is the wavelength of the X-ray, where it is 0.154 nm. K is 0.89 when θ_{hkl} takes the half of the broadening of the diffract peak. The particle sizes corresponding to the (111), (200), and (220) diffract peaks were calculated, and the average sizes of samples A_0 , B_0 , and C_0 are 27.6, 22.0, and 6.0 nm, respectively. Based on the calculated results, it can be seen that the sample C_0 has a smaller particle size than

the others, which implies that there may exist more growth defects and grain boundaries [13].

To investigate the surface morphology of ZnS samples, the authors took a small part of the samples and coated them on the conductive adhesive to perform the SEM observation. It is found that the samples A₀ and B₀ grown from different zinc source have nearly the same morphologies, as displayed in Fig. 2a and b. Both samples show densely distributed nanoparticles with rough surfaces. The average particle sizes measured from SEM images are about 40 and 50 nm for the samples A₀ and B₀, respectively. While perfectly sphere-like shapes with the diameters in the range of 2–3 μm were found on the surface of sample C₀ (Fig. 2c). It is worth noting that the size determined by SEM is much larger than the calculated results by the Scherrer equation. The remarkably difference indicates that the spheres are the aggregation of the initially formed ZnS nanocrystals [14, 15]. This is not the case for the samples A₀ and B₀, where the particle sizes from the SEM are just lightly larger than those calculated by the Scherrer equation. It is important to realize that the Scherrer equation provides a lower bound on the particle size, because a variety of factors can contribute to the width of a diffraction peak, such as inhomogeneous strain, instrumental effects, and the lattice imperfection in the crystal.

It is well known that ZnS nanostructures are promising for light-emitting applications due to their efficient visible luminescence in the 2–4 eV region. The room temperature PL spectra of the as-prepared ZnS nanostructures taken under excitation with the 325 nm line of the He–Cd laser are displayed in Fig. 3. The PL spectra for the three samples all show a broad emission band ranging from 400 to 650 nm. It can be seen that the PL peak positions are constant at 525 nm for the three, and the emission intensity changes greatly. It implies that the PL originates from the same defect center and there exists a great difference in the

defect contents. Previously, Bol and Meijerink [16] reported that the nanocrystalline ZnS doped with Cu²⁺ and Mn²⁺, or other rare earth ions can show a visible region emission from blue to green. However, it is unlikely that the emission of the present ZnS nanostructures is related to donor impurity levels in view of its high-purity ZnS reagents used. Energy dispersive X-ray spectrum (EDS) (Fig. 3b) from the products show detailed information about the chemical compositions. The presence of sulfur, zinc, and silicon were identified. The signal of silicon comes from the Si substrate. Recently, Tsuruoka et al. [11] ascribed the green emission band located around 535 nm to the line or planar defects of the ZnS nanobelts. In the experiments, the as-prepared samples, both nanoparticles and nanospheres are of polycrystalline phase, where no similar line and planar defects existing as those in the nanobelts. Therefore, the line and planar defects are excluded as the origin of the green band. Ye et al. [17] and Shen et al. [18] concluded that the elemental S species on the surface of the ZnS nanobelts (nanowires) contribute to the green PL band. However, it is noteworthy that the PL position is not very sensitive to the change of the surface structure (nanoparticles and nanospheres). So, there should be another reason for the observed green band. Becher et al. [19] calculated the band structure of ZnS and predicted that many self-activated point defects such as Zn vacancies within the band gap. In this experiment, the green PL intensity decreased greatly with increasing the nanoparticles size of the as-prepared samples. Combined with the preparation processing of the three samples, it is reasonable to believe that the PL band centered at 525 nm in the ZnS nanostructures originates from the zinc vacancies. In fact, it is very likely to introduce vacancies-related defects for the experiments were carried out at a relatively low temperature. Hence, more zinc vacancies exist in the products, as proved by many theoretical and experimental reports

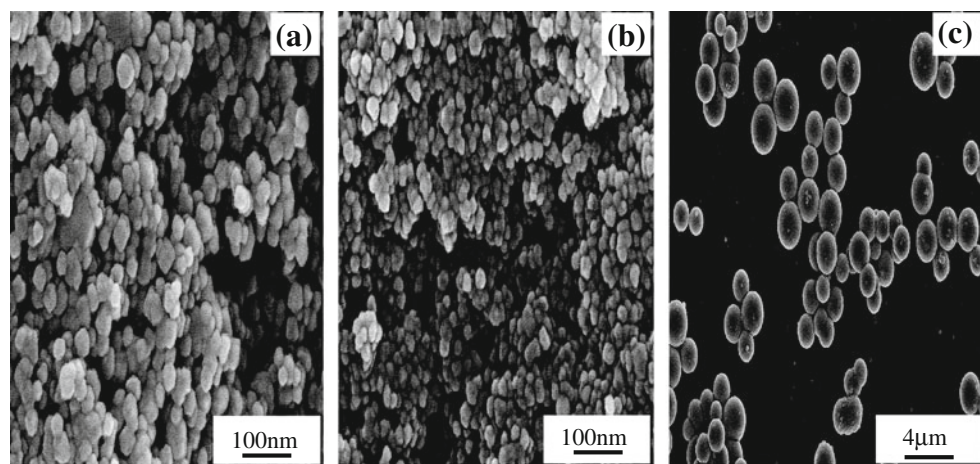


Fig. 2 SEM images of **a** sample A₀, **b** sample B₀, and **c** sample C₀

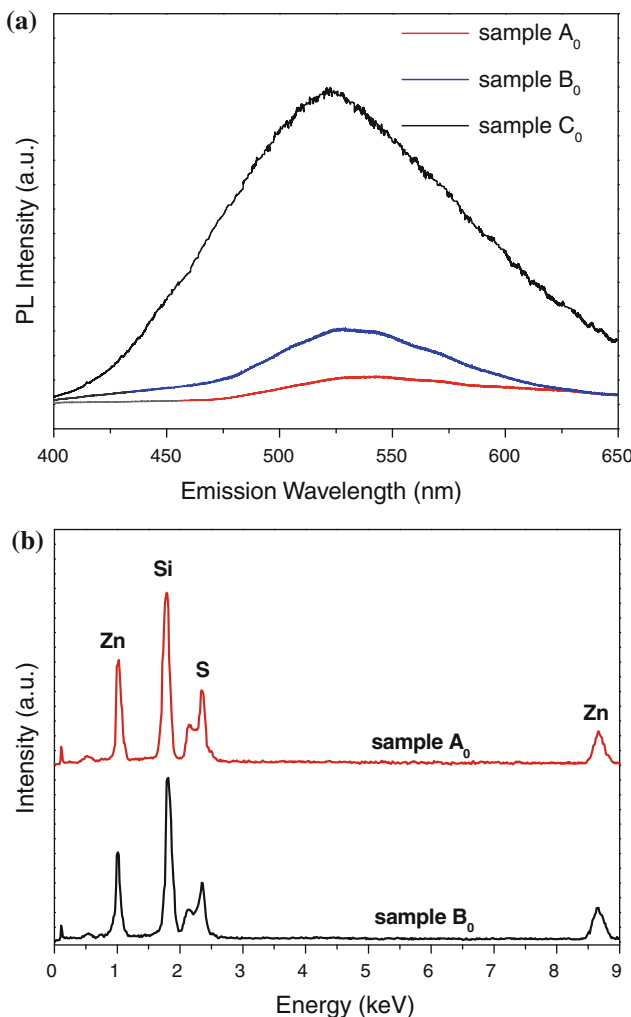


Fig. 3 **a** PL spectra of the samples A₀, B₀, and C₀, taken under excitation with a 325 nm line of He–Cd laser. **b** Energy dispersive X-ray spectrum of sample A₀ and B₀

[20–23]. As for the great change in intensity of PL from samples A₀, B₀, and C₀, it is because that the reduced size leads to an exceptionally high surface area and creates a remarkable increase in the zinc vacancies near the surface. In the experiments, the average particle size values of sample A₀, B₀, and C₀ are 27.6, 22.0, and 6.0 nm. Moreover, it should be noted that the PL is very sensitive to the change of surface morphology. In this experiment, the authors did not observe any visible change in the PL spectra for the nanoparticle and sphere-like ZnS nanostructures, which further supports the defect related origin of the green emission.

To confirm the inference about the positions of zinc vacancies, the authors synthesized more samples with different ratios (1.2:1, 1:1, 1:1.2, 1:1.5) of zinc and sulfur using zinc acetate as the zinc source and thiourea as the sulfur source and then examined their PL spectra, as shown

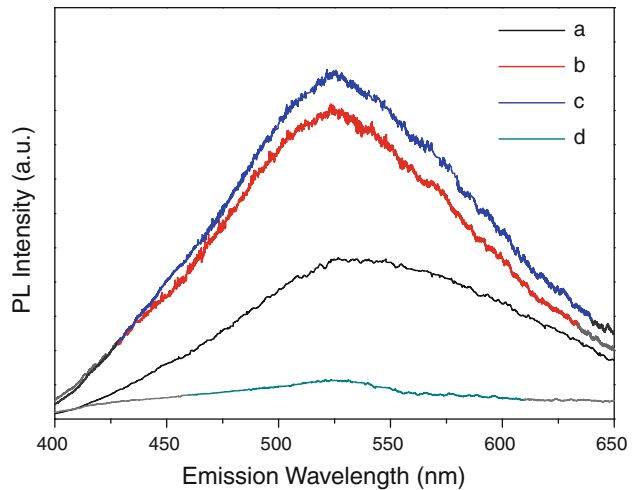


Fig. 4 PL spectra of the samples with different ratios of zinc and sulfur. **a** 1.2:1. **b** 1:1. **c** 1:1.2. **d** 1:1.5

in Fig. 4. If the zinc vacancies in the samples of the ZnS nanostructures are indeed responsible for the green PL band, the intensity of this band should decrease with increasing the zinc contents, which was successfully proved by the experimental results. One can see that the PL intensity in Fig. 4 obviously decreases with increasing the Zn:S ratio. On the basis of these results, the authors can conclude that the self-activated zinc vacancies point defects of the ZnS nanostructures do contribute to the green PL band. The luminescence centers are formed when zinc vacancies are introduced into the ZnS nanostructures, which lead to the detected green emission from the ZnS nanostructures. It also can be seen that there is a little shift in the PL peak positions. It is because that the different ratios of the zinc and sulfur will cause a little change in the size of the four samples. For the quantum confinement effects, the different sizes will bring an impact on the band gap of the samples and cause a little shift in the PL peak positions [24].

Conclusions

In conclusion, the authors have solvothermally fabricated ZnS nanoparticles and nanospheres for clarifying the origin of the green PL band. The PL intensity reduced greatly with increasing the nanoparticle size and the ratio of zinc and sulfur sources in the preparation process. Spectral examinations and analyses reveal that the green emission band from ZnS nanostructures indeed originates from the self-activated zinc vacancies points of the ZnS nanostructures. This experiments and results will be beneficial to the understanding of light-emitting mechanisms in various ZnS nanostructures.

Acknowledgements This study was jointly supported by the Natural Science Foundation of Jiangsu Province (Grant no. BG2007026) and the National Natural Science Foundation of China (Grant no. 11004170).

References

1. Shen GZ, Bando Y, Hu JQ, Golberg D (2007) *Appl Phys Lett* 90:123101
2. Yamamoto T, Kishimoto S, Iida S (2001) *Physica B* 308:916
3. Becker WG, Bard AJ (1983) *J Phys Chem* 87:4888
4. Meng XM, Liu J, Jiang Y, Chen WW, Lee CS, Bello I, Lee ST (2003) *Chem Phys Lett* 382:434
5. Ye C, Fang X, Li G, Zhang L (2004) *Appl Phys Lett* 85:3035
6. Rosenberg RA, Shenoy GK, Heigl F, Kim PSG, Zhou XT, Sham TK (2005) *Appl Phys Lett* 87:253105
7. Dunstan DE, Hagfeldt A, Almgren M, Siegbahn HOG, Mukhtar E (1990) *J Phys Chem* 94:6797
8. Jiang Y, Meng XM, Liu J, Xie ZY, Lee CS, Lee ST (2003) *Adv Mater* 15:323
9. Qi L, Lee BI, Kim JM, Jang JE, Choe JY (2003) *J Lumin* 104:261
10. Zhao Q, Hou L, Huang R (2003) *Inorg Chem Commun* 6:971
11. Tsuruoka T, Liang CH, Terabe K, Hasegawa T (2008) *Appl Phys Lett* 92:091908
12. Gode F, Gumus C, Zor M (2007) *J Cryst Growth* 299:136
13. Chen HT, Wu XL, Zhang YY, Zhu J, Cheng YC, Chu PK (2009) *Appl Phys A* 97:581
14. Tong H, Zhu YJ, Yang LX, Li L, Zhang L, Chang J, An LQ, Wang SW (2007) *J Phys Chem C* 111:3893
15. Jiang LF, Yang M, Zhu SY, Pang GS, Feng SH (2008) *J Phys Chem C* 112:15281
16. Bol AA, Meijerink A (2001) *J Phys Chem B* 105:10197
17. Ye CH, Fang XS, Li GH, Zhang LD (2004) *Appl Phys Lett* 85:3035
18. Shen GZ, Bando Y, Golberg D (2006) *Appl Phys Lett* 88:123107
19. Becher WG, Bard AJ (1983) *J Phys Chem* 87:4888
20. Mistui T, Yamamoto N, Tadokoro T, Ohta S (1996) *J Appl Phys* 80:6972
21. Denzler D, Olschewski M, Sattler K (1998) *J Appl Phys* 84:2841
22. Hu JQ, Bando Y, Zhan JH, Golberg D (2005) *Adv Funct Mater* 15:757
23. Zhang YG, Lu F, Wang ZY, Wang HX, Kong MG, Zhu XG, Zhang LD (2007) *Cryst Growth Des* 7:1459
24. Chen HT, Xing SJ, Wu XL, Zhu J, Shen JC, Chu PK (2009) *Nano Lett* 9:1926